Desalination and Water Treatment
www.deswater.com
doi: 10.1080/19443994.2016.1186569

57 (2016) 28176–28186
December

Taylor & Francis
Taylor & Francis Group

Revised spacer design to improve hydrodynamics and anti-fouling behavior in reverse electrodialysis processes

Zhaolong He[a,b], Xueli Gao[a,b,*], Yushan Zhang[c], Yuhong Wang[d], Jian Wang[a,b]

[a]*Key Laboratory of Marine Chemistry Theory and Technology, Ministry of Education, Qingdao 266100, China, Tel./Fax: +86 0532 66782017; email: gxl_ouc@126.com (X. Gao)*
[b]*College of Chemistry & Chemical Engineering, Ocean University of China, Qingdao 266100, China*
[c]*Institute of Tianjin Desalination and Multipurpose Utilization, State Oceanic Administration, Tianjin 300192, China*
[d]*National Center of Ocean Standards and Metrology, Tianjin 300112, China*

Received 17 December 2015; Accepted 8 April 2016

ABSTRACT

Reverse electrodialysis (RED) is a technology to obtain energy from mixing waters with different salinity. Small intermembrane distances and high flow velocities are preferred to obtain high power generating capacity accompanying high power consumption, however. To increase power generation without redundant power consumption, we designed a new water feeding pattern system. The new water feeding pattern was designed to configure additional water inlet and outlet, instead of single inlet and outlet. The experimental results showed that the new design was beneficial to promote the flow distribution, thus reduced the solution resistance compared to the traditional water feeding pattern system. The net power density in the new water feeding pattern system increased by 36.4% than that in the previous system. Results of fouling-resistant experiments also demonstrated that the RED stack with the new water feeding pattern showed significantly less sensitivity to fouling under natural conditions and a 20-d operation than the traditional one. These results suggest that the new spacer design is very effective to obtain higher power density and simultaneously reduce the membrane fouling tendency.

Keywords: Reverse electrodialysis; Salinity difference; Power density; Fouling; Feeding pattern

1. Introduction

Reverse electrodialysis (RED) is one of the membrane processes that captures energy from mixing waters with different salinity, for example, where river water is discharged into the sea [1]. The mixing of waters with different salinity could generate a huge amount of energy (1.9–2.6 TW) [2–5], even much smaller than that generated by wind (10TW) and solar (3.6×10^4), which could meet the worldwide electricity requirement [6,7]. In a RED system, stacks of alternating ion selective are used to separate the high concentration (salt water) from the low concentrate (fresh water). Then, a gradient in chemical is created by this separation, which generates a Donnan or membrane potential when waters with different salinity are on either side of anion and cation exchange membrane. As the number of membranes in the RED stack increased, the membrane potential increases and drives an electrochemical redox reaction [8,9] at electrodes and ultimately generate electricity.

*Corresponding author.

In traditional designs of RED, the power density is associated with the spacers thickness [10,11] and the flow velocities on the membrane surface [12]. The distance between the membranes is determined by the spacers, which restrict the capacity and energy consumption of RED stack. To reduce the loss of power generation, RED stacks are designed to have thin spacers and compartments. The flow velocities are higher within the thinner spacers, which can reduce the generation of dead zones and generate a more uniform flow distribution. The greater distribution of the solution in the compartments will promote the mixing of salinity in the compartments, which can reduce the concentration difference between the membrane surface and the bulk solution and finally resulted in a smaller electric resistance. The traditional and thin spacers reduce the electric resistance of feed water compartment by generating a more uniform flow distribution [13], but the power consumption of the pump is high. Długołeckia et al. [14] presented results of her laboratory investigations of RED, she designed ion conductive spacers to replace the traditional spacers. Experiments showed that these ion conductive spacers led to a decrease in stack resistance and an increase in power density than the design with the traditional spacers.

The fouling in RED has an important influence on the permselectivity of the membranes and the obtained power density, the biological fouling can also lead to an increase in pressure drop for pumping the feed waters. The effect of fouling on performance can be quantified and measured by Energy Dispersive X-ray spectroscopy (EDX), the change of pressure and power density with time. Post (2009) studied a setup without spacers and Vermaas et al. [15,16] (2011) designed a setup through using the profiled membranes to substitute the use of spacers showed less sensitive to fouling. The transformation of the membranes is rather difficult to achieve through technical means. When using spacers between the membranes, the different flow velocities on membrane surface will cause a different residence time, thus the flow velocity is lower where pollution is more serious. Thus, our goal is to reform the spacers under the theoretical basis and achieve improved power energy with little membranes fouling.

In this work, we design a new water feeding pattern and investigate the potential of the application of new spacers in RED to reduce the solution resistance. We systematically study the new feeding pattern system (NFPS) and traditional feeding pattern system (TFPS) on the stack voltage, stack power density, flow field analysis, and membrane fouling. It is observed in RED when the new spacers are used and significantly increase the power density obtainable in RED. This study is contributive to the knowledge and discussion on spacers and hydrodynamics, which make the RED more specific.

2. Material and methods

2.1. Experimental setup

The RED stack consists of three circulating systems and each system comprises a tank, a flow-meter, a manometer, and a circulation pump [17,18]. Each circulation pump could give a needed circulation flow during the process. The RED stack equipped with 9 anion and 10 cation exchange membranes (CEM), giving 9 diluting and 9 concentrating compartments that correspond to 9 unit cells. This process is illustrated in Fig. 1. The membrane size was 200 mm × 120 mm and the effective membrane area was 110 cm^2. The flow velocity was controlled by flow-meter. The conductivity and temperature of the influent and effluent were measured by conductivity meter (METTLER TOLEDO FE30) and recorded every minute. The open circuit voltage (V), the electric resistance, and the power density of the RED stack were monitored every minute using chronopotentiometry (Zahner, The Germany).

In this experiment, the homogeneous anion exchange membranes (AEM) and CEM were supplied by Qianqiu Environmental Protection & Water Treatment Corporation, China. The homogeneous monovalent-selective anion exchange membranes (1-AEM) were supplied by Asahi Glass Company, Japan. The main characteristics were detailed in Table 1.

2.2. Feed waters

In this experiment, artificial solutions of 0.508 M NaCl (30.0 g NaCl per kg water) and 0.017 M NaCl (1.00 g NaCl per kg water) were used as seawater and river water, respectively [19]. The feed waters were pumped through the stack at 4 different flow velocities between 0.38 and 1.04 cm/s [20]. In order to study membrane fouling, the stacks of NFPS and TFPS were fed continuously with natural seawater and river water at a flow velocity of 0.58 cm/s (20 d). The river water was obtained from a nearby river (Li Cun) and sea water was obtained from the nearby harbor in the Yellow Sea.

To facilitate an electric current, the electrodes (Ti meshed, coated with Ir/Ru) were supplied with $FeCl_3$ and $FeCl_2$ solutions in this test. By applying the 1-AEMs as outer membranes, the Fe^{3+} and Fe^{2+} were kept in the electrode compartment. At the same time, Fe^{3+} and Fe^{2+} were limitless to convert to each other for generating an electromotive force without adding new electrolyte solution of $FeCl_3$ and $FeCl_2$.

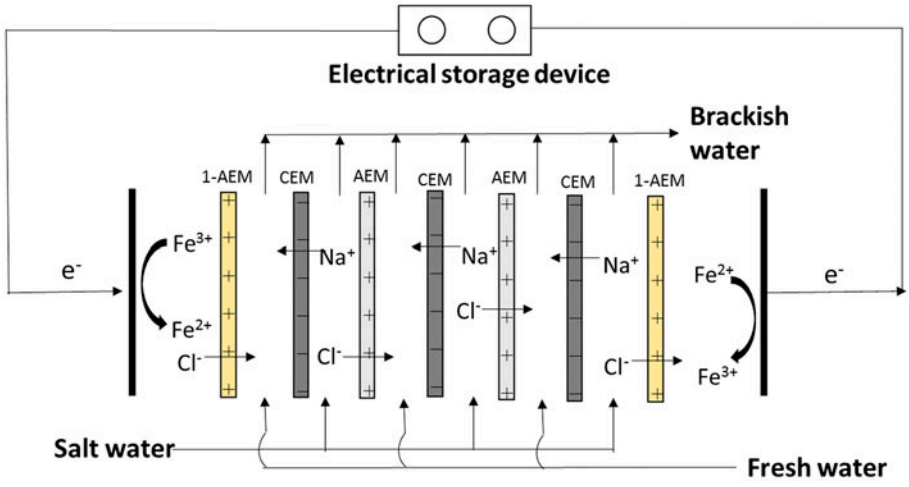

Fig. 1. Principle of RED system. Membrane potential is generated when waters with different salinity are on either side of anion and cation exchange membrane. A reversible redox reaction about Fe^{3+} and Fe^{2+} converts the ionic current into an electric current.

Table 1
Main characteristics of the anion- and cation-exchanged membranes

Membrane	Thickness (mm)	IEC (meq/g)	Area resistance (Ω cm^2)	Selectivity (%)
AEM	0.16–0.23	1.8–2.0	5–9	>95
CEM	0.16–0.23	2.0–2.2	2–5	>97
1-AEM	0.12–0.15	1.7–2.3	3–12	>97

2.3. Spacers

The new water feeding pattern is depicted in Fig. 2, which allows the feed water to distribute in the RED stack. The new spacer and the traditional spacer are shown in Fig. 3 for the case with a different way of water feeding. The new spacer is superior to the traditional spacer for hydraulic characteristics, which is optimized at the same flow velocity. At the same time, the electric resistance in the RED stacks is lower when using the new spacers than the traditional spacers. The RED stacks with the new spacers can promote mixing and flow distribution in the compartments without high power consumption of the pump. The characteristics of the spacers are listed in Table 2.

2.4. Analysis method

Chronopotentiometry was applied to benchmark the obtained power density in each RED stacks. A galvanostat (Zahner, The Germany) was used to measure the voltage at different current densities of 1, 2, 3, 4, 5, 6, 7, 8, and 9 A/m^2. To ensure a stable voltage, during the measure, at least four times of the residence time for the feed water was used. The measurements were performed at different feeding solutions of electrolyte. Each stage in current density was preceded and followed by stage with open circuit voltage. The stack load resistance (R_L, in Ω cm^2) was associated with the diffusion boundary layer which included the internal (R_{int}) and external resistance (R_{ext}) [20]. The internal resistance originates the total membrane ($R_{membrane}$) and solution resistance ($R_{solution}$) within the stack [21,22]:

$$R_L = R_{int} + R_{ext} \quad (1)$$

$$R_{int} = R_{membrane} + R_{solution} \quad (2)$$

$$R_{solution} = R_{sea} + R_{river} \quad (3)$$

The AEM and CEM have area resistance (Table 1), which remain basically unchanged. The solution resistance (R_{river} and R_{sea}) is calculated from the molar conductivity Λ_m of the feed water. The river water resistance plays a dominant position of the total solution resistance, because Λ_m is dependent on the concentration C:

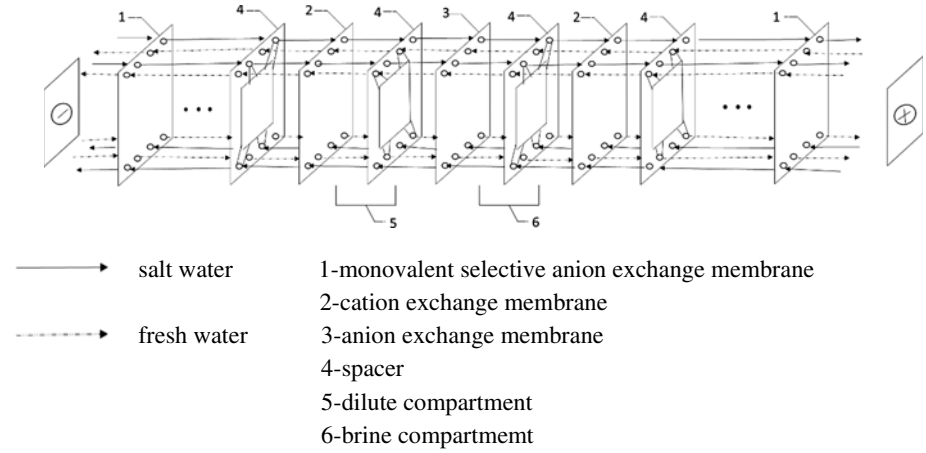

Fig. 2. The new water feeding pattern of laboratory RED stack.

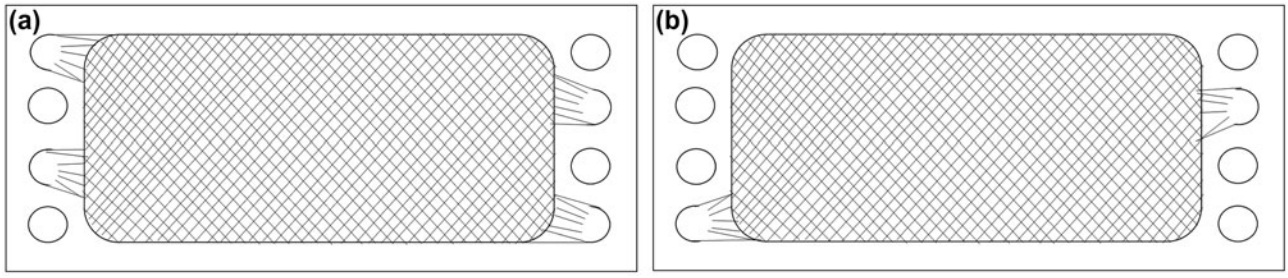

Fig. 3. The spacers of the new water feeding pattern (a) and the traditional water feeding pattern (b) in the RED stack.

Table 2
Main characteristics of the spacers

Spacers	Thickness of net (mm)	Thickness of frame (mm)	Porosity, ε (%)	Materials	Manufacturer
	0.45	0.72	86.5	Polypropylene	Tianwei Membrane Technology Co., Ltd

$$R_{sea} = f\frac{\delta_s}{\Lambda_m C_s} \quad (4)$$

$$R_{river} = f\frac{\delta_r}{\Lambda_m C_r} \quad (5)$$

In the equations of (3) and (4), the δ_s and δ_r are the thicknesses of the sea and river water compartment. The f is an obstruction factor of the spacers (tortuosity of the ion path, shielding the membranes and the decrease in conducting solution). So, the sum resistance associated with the diffusion boundary layer, the process of feed water flow and the concentration changes of each compartment. The concentration difference over the membranes will decrease when the ions transport from the salt water compartment to the fresh water compartment and this can be accelerated by disturbance effect of the new feeding pattern.

The theoretical voltage that is generated by the salinity gradient can be calculated by the Nernst equation:

$$V = N_m(t_K + t_A - 1)\left(\frac{RT}{nF}\right)\ln\left(\frac{a_{sea}}{a_{river}}\right) \quad (6)$$

In which, t_K and t_A are the apparent transference number of the CEM and AEM, respectively, R is the universal gas constant (8.314 J/(mol k)), T is the absolute temperature (K), F is the Faraday constant (96,485 C/mol), n is the valence of the ion species (–), a_{sea} and a_{river} are the activities of the seawater and river water, respectively.

The power output P (W/m^2 of membrane area) is calculated from the circuit voltage (V) and the stack load resistance:

$$P = \frac{V^2}{R_L wl} \tag{7}$$

In which, w is the stack width and l is the stack length. Noted that the maximum power output P (W/m^2 of membrane area) can be calculated from the circuit voltage (V) and the stack load resistance [20].

This paper focuses on the power generation from salinity gradients, as the internal resistance influences the power density. The power density can be enhanced by reducing the internal resistance.

2.5. Mass transfer in the diffusive boundary layer

Transfer process on the membranes surface is considered within the scope of the so-called boundary-layer (δ) model, which assumes that within a boundary film adjacent to the membrane interface, the solute transport occurs concentration diffusion, electric migration, and convection in the direction normal to the membrane surface, alone. The fluid velocity in boundary layer is gradual, the fluid speed of the membranes surface is zero, and the flow velocity of the outer edge of the boundary layer close to the velocity of feeding water. Outside this boundary layer, the concentrations of all the ions are assumed to be homogeneous because of fast mixing. The boundary layer is defined as Eq. (9) due to the same order of magnitude of viscosity and inertia force, Eq. (8) takes this very simple form:

$$\mu \frac{U_\infty}{\delta^2} \sim \frac{\rho U_\infty^2}{L} \tag{8}$$

where

$$\delta \sim \sqrt{\frac{\mu L}{\rho U_\infty}} \tag{9}$$

where μ is the coefficient of viscosity, ρ is the solution density, L is the length of membranes, and U_∞ is the speed of feeding water. From this equation, we can get that the thickness of boundary layer (δ) is in inverse proportion to the square of speed of feeding water (U_∞). Hence, the thickness of boundary layer (δ) will be thin with the increase in speed of feeding water on the membranes.

At steady state, and according to boundary-layer theory, the migration of ion i in the boundary layer can generally be expressed by the following Nernst–Planck equation:

$$J_i = D\frac{\mathrm{d}c_i}{\mathrm{d}x} + \frac{FD_i c_i z_i}{RT}\frac{\mathrm{d}\Psi}{\mathrm{d}x} + c_i U \tag{10}$$

where

$$\left(\frac{\mathrm{d}c}{\mathrm{d}x}\right)_{x=0} = \frac{c_\mathrm{m} - c_0}{\delta} \tag{11}$$

$$t_i = \frac{J_i}{J} \tag{12}$$

where J_i is the transfer flux of ion i, D is the diffusion coefficient for the electrolyte; c_i, D_i, and z_i are the concentration, diffusion coefficient, and charge number of ion i; F is faraday constant, R is the gas constant, and T is the temperature in K; Ψ is the electric potential and U is the speed of water. From this equation, we can know that the transfer flux (J_i) will be higher with the increase in speed of water on the membranes. This means that, in this situation, the apparent transference number (t_i) will get higher which will cause the increase in the power output (P) by Eqs. (6) and (7).

3. Results and discussion

3.1. The voltage of RED with TFPS and NFPS

RED performance was preliminarily checked by feeding fresh (0.017 M NaCl) and sea water (0.5 M NaCl). The voltage is an important parameter often used to characterize the maximum power output obtainable in processes such as RED or fuel cells. The stack consists of 9 cell pairs, each consisting of an anion and a CEM with an effective membrane area of 110 cm^2 per membrane. The theoretical value of the stack voltage can be calculated by the Nernst equation and for fresh (0.017 M NaCl) and sea water (0.5 M NaCl), this theoretical voltage difference over each membrane for 100% selective membranes is 0.08 V [23]. The average membrane permselectivity can be calculated as the ratio of experimentally and theoretical stack voltage multiplied by 100%. The calculated permselectivity is closely related to experimentally determined membrane perm selectivity.

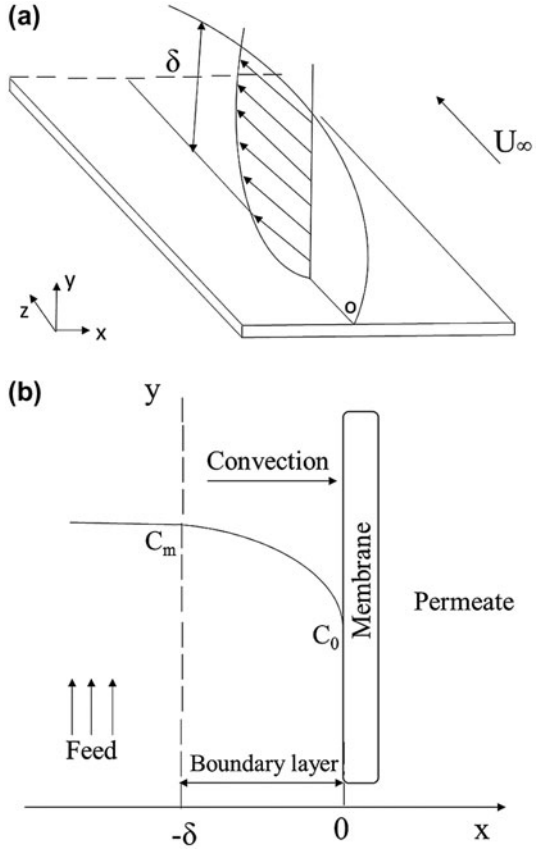

Fig. 4. The schematic diagram of boundary layer considered here (a) and the boundary layer conditions at the membrane (b).

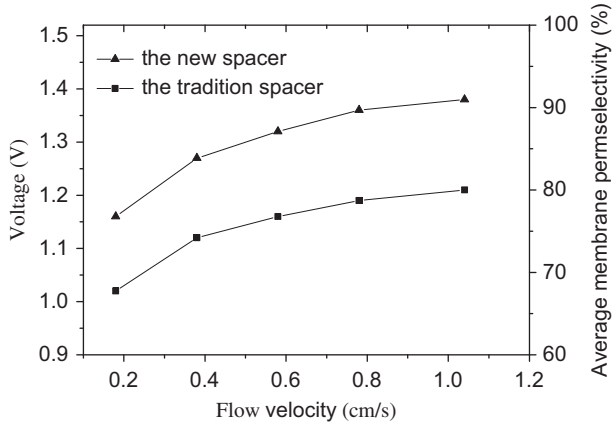

Fig. 5. Voltage of the RED stack and the average membrane permselectivity as a function of the solution flow velocity for different spacers in the stack.

This membrane permselectivity is shown as well in Fig. 4 (second *y*-axis).

Fig. 5 shows that the stack voltage values for the new spacers are higher than the values obtained for the tradition spacers. This is due to the occurrence of concentration polarization phenomena, which may play bigger role when tradition spacers are used. The phenomena of concentration polarization occur not only on the membrane–solution interface, but also on the spacer–solution interface. The concentration polarization phenomena are low when the hydrodynamic conditions are optimal in the stack. Due to the occurrence of more severe concentration polarization phenomena at the membrane–solution and spacer–solution interface when the tradition spacers are used in RED stack, resulting in a lower experimental voltage and therefore lower average membrane permselectivity.

3.2. The effects of the RED operation conditions on power density

3.2.1. The influence of flow velocities (NFPS)

The concentration of electrolyte solutions (the mixing $FeCl_3$ and $FeCl_2$) is set to 0.25 M in this experiment. The experimentally obtained power density is shown in Fig. 6 as function of the current density for different flow velocities. It can be seen from Fig. 6 that the maximum power density increase from 0.37 to 0.533 W/m^2 with the flow velocity increasing from 0.38 to 1.04 s/cm, which indicates that the flow velocity has a significant influence on the power density. For low flow velocities, ion transport from seawater compartments to river water compartments is slow, which makes the power density low [24,25].

Each power density curve can be divided into two sections: the first portion where the stacks perform similarly (low current); and the second portion where stack performance differs (high current) [26]. At low

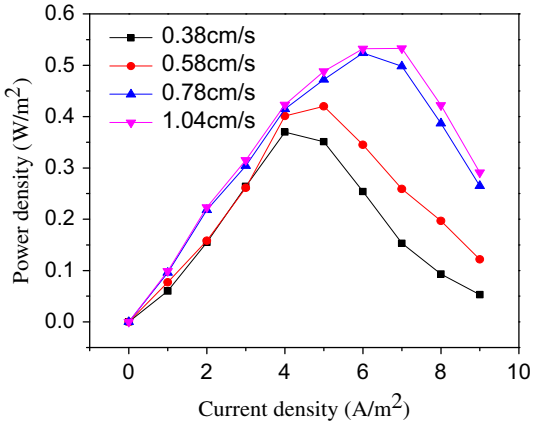

Fig. 6. Relationship between the current density and power density at different flow velocities with new spacers.

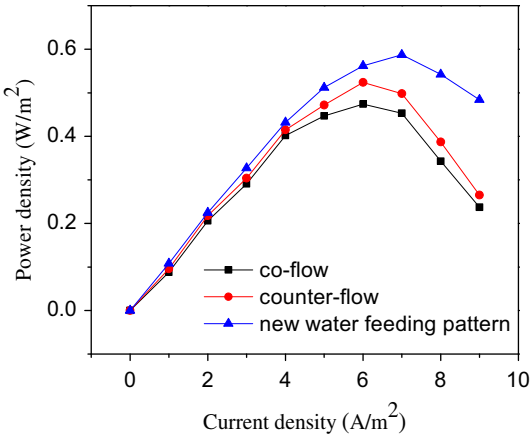

Fig. 7. Influence of feed pattern on power density at the flow velocity of 0.78 cm/s.

current, only small deviations in power density were observed. It can be concluded that current density plays a major role to power density at low current than flow velocities. The turning point of the power density curve was different under different flow velocities. At high flow velocities, this occurred at 7 A/m^2 and at low-flow velocities, this occurred at 4 A/m^2.

3.2.2. The influence of water feed pattern

The concentration of electrolyte solution of the mixing ($FeCl_3$, $FeCl_2$) is 0.25 M in this experiment. Fig. 7 presents that the power density curve first increases and then decreases with the increasing in current density at the constant flow velocity. The new water feeding pattern is shown in Fig. 3 for the case with two inflows and two outflows. The highest power density is obtained for the RED stack with the new water feeding pattern, whereas the RED stack with the co-flow performed the worst. This is due to the more distribution of the compartments, which can be optimized by higher flow velocities and the new water feeding pattern, compared to the traditional water feeding pattern. The greater distribution of the solution in the compartments will promote the mixing of salinity in the compartments, which can reduce the concentration difference between the membrane surface and the bulk solution. So the more distribution of the compartments can reduce the concentration polarization effects. Therefore, the solution resistance is lower for the RED stack with the new water feeding pattern to that with co-flow and counter flow. In addition, the resistance of water feeding is lower with the new water feeding pattern than that of co-flow and counter flow.

The power density curve fall more slowly under the new water feeding pattern than that of co-flow and the counter flow. This is because the new water feeding pattern ensures a more uniform feed water distribution over the membrane area, while the traditional inflow and outflow of the RED stack as in previous research can create more preferential channeling and dead zones. Therefore, the power density curve could show smoother under the new water feeding pattern than the co-flow and the counter flow after the turning point.

3.2.3. The comparison of NFPS and TFPS under natural water and artificial water

The new spacer and the traditional spacer are shown in Fig. 3 for the case with a different way of

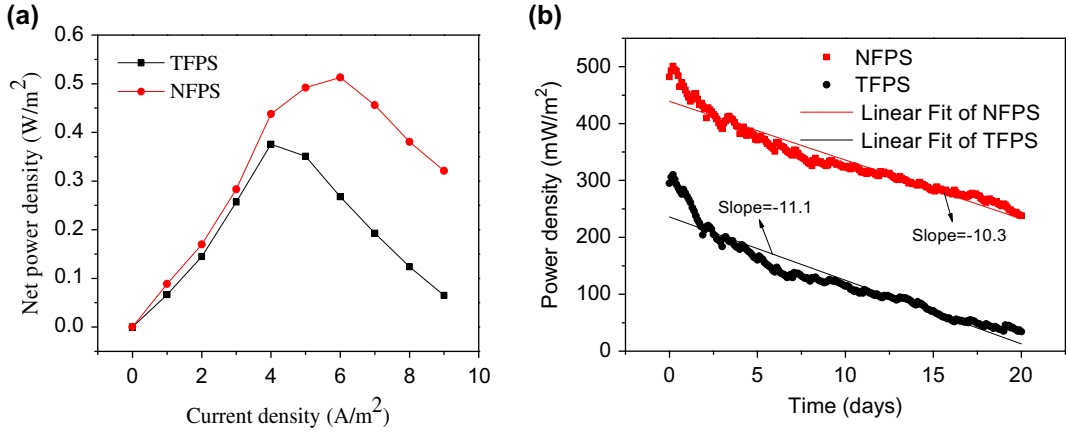

Fig. 8. Influence of spacers on net power density under artificial water (a) and the change of power density under natural water with 20 d (b).

water feeding. The concentration of electrolyte solution of the mixing ($FeCl_3$, $FeCl_2$) is 0.25 M. It can be seen from Fig. 8(a) that the 36.4% more net power density with the new spacer than the traditional spacer can be obtained at the same flow velocity of 0.78 cm/s. Compared to the traditional water feeding pattern, the new spacer is beneficial to make water distribute equably in the compartments at the same flow velocity. The hydraulic characteristic with the new spacer was better than the traditional spacer in the RED stack.

The time series for power density change under natural water, for all systems, are presented in Fig. 8(b). For the stack with the new spacers, the power density declined much slower than that of traditional spacers. It can be seen that the power density decline slow with time under all systems. The slower decline in power density in the stack with the new spacers, compared to the stack with the traditional spacers, can be explained by the uniform distribution of the feed water. It is easy to form a channel between the compartments when using the traditional spacers in the stack. Bacteria and insoluble solids are easily deposited on the membranes, which let the power density decline in the stack under TFPS. The uniform distribution that is created by the new spacers gives less opportunity for bacteria and insoluble solids to attach, and consequently gaining higher power density than using the traditional spacers.

3.3. Flow field analysis using computational fluid dynamics

Fig. 9 shows that the flow bends around the new spacers and traditional spacers at the flow velocities of 2, 3, and 4 cm/s. The flow velocities with the new spacers are more uniform than that of traditional spacers. Compared to the traditional spacers, the flow velocities with the new spacers are higher at the same position of spacer. Therefore, the RED stack with the traditional spacers can form channel flow more easily than that of new spacers, which has higher electric resistance.

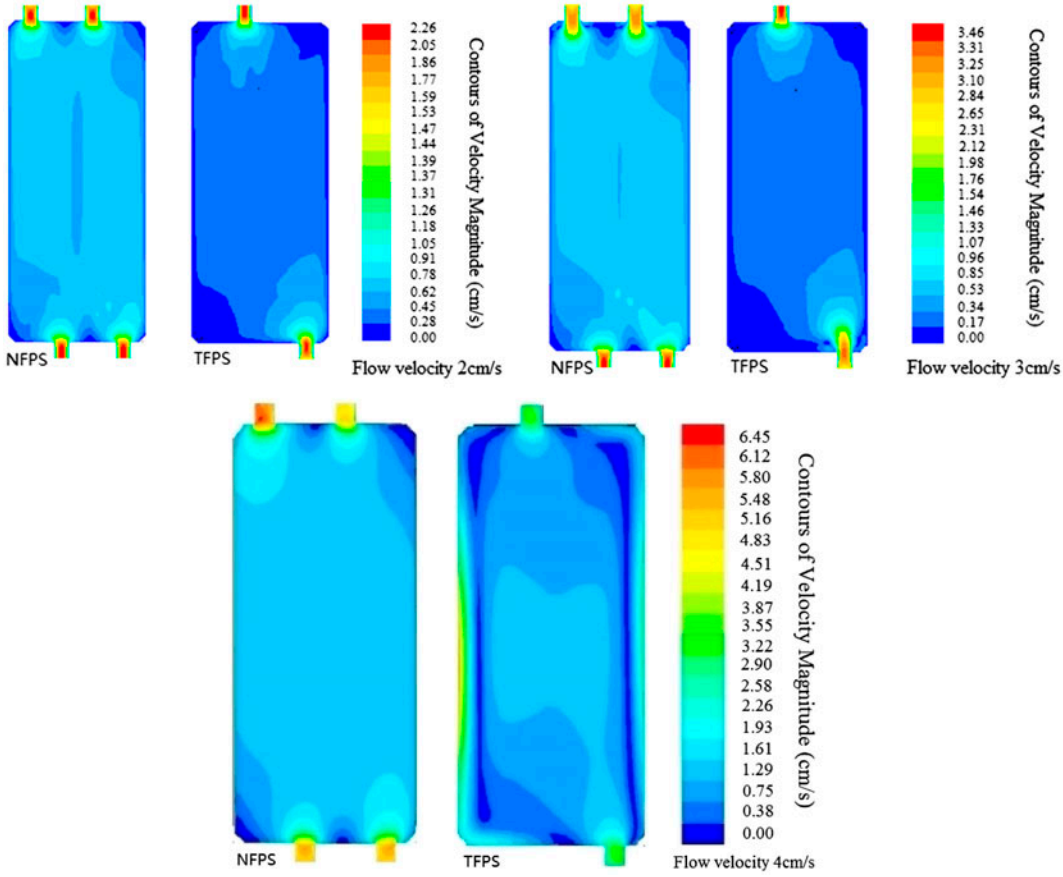

Fig. 9. CFD analysis at different flow velocities (2, 3, and 4 cm/s) with the new spacers and the traditional spacers in the RED stack.

This computational fluid dynamics (CFD) analysis demonstrated that the performance of the new spacers was superior to the traditional spacers [27]. Non-uniform flows bend around the traditional spacers can accentuate concentration polarization effects at the membrane surface and increase the membrane resistances compared to the new spacers design. The flows bend around the traditional spacers form dead zones, which cause a significant decrease in performance and increase the accumulation of bubbles, reducing the active membrane area available for ion diffusion.

3.4. Visual and microscopic inspection of membranes with NFPS and TFPS

The membranes of all systems were investigated visually by SEM-EDX after 20 d operation. The anion exchanged membranes (AEMs) had turned yellowish (originally white). In comparison to NEPS, the membranes' color with TFPS was deeper. The color of cation-exchanged membranes (CEMs) has little change and preserves their original beige color.

Fig. 10 shows some representative images of the fouled membranes samples from all systems which are inspected with SEM. These images show that all samples under NFPS and TFPS are covered with a mixture of deposits. The SEM images clearly demonstrate that the CEMs are covered with less deposition than the AEMs under all systems. The CEMs and AEMs under NFPS are optically less fouled, except for the corner of the membranes, because this part can easily form dead zones. The CEMs and AEMs under TFPS are covered with mass deposits and bacteria, and most of them have the form of aggregate. This phenomenon was in agreement with the result shown in Fig. 10. The formation of pollutants on the membranes is spreading over a whole area from one point, and the uneven surface of the membranes will lead to the aggregate increase of pollutants, such as the fouling of the CEM under TFPC (b-2).

The composition of these membranes is investigated using EDX for all samples. The result of elemental analysis (expressed as atomic percentage %) of membranes is listed in Table 3. The results of EDX appear high carbon content, which contains significant amounts of the membrane. The concentration of magnesium, calcium, and phosphorus are typically higher on the CEMs, indicating that the CEMs are easier to

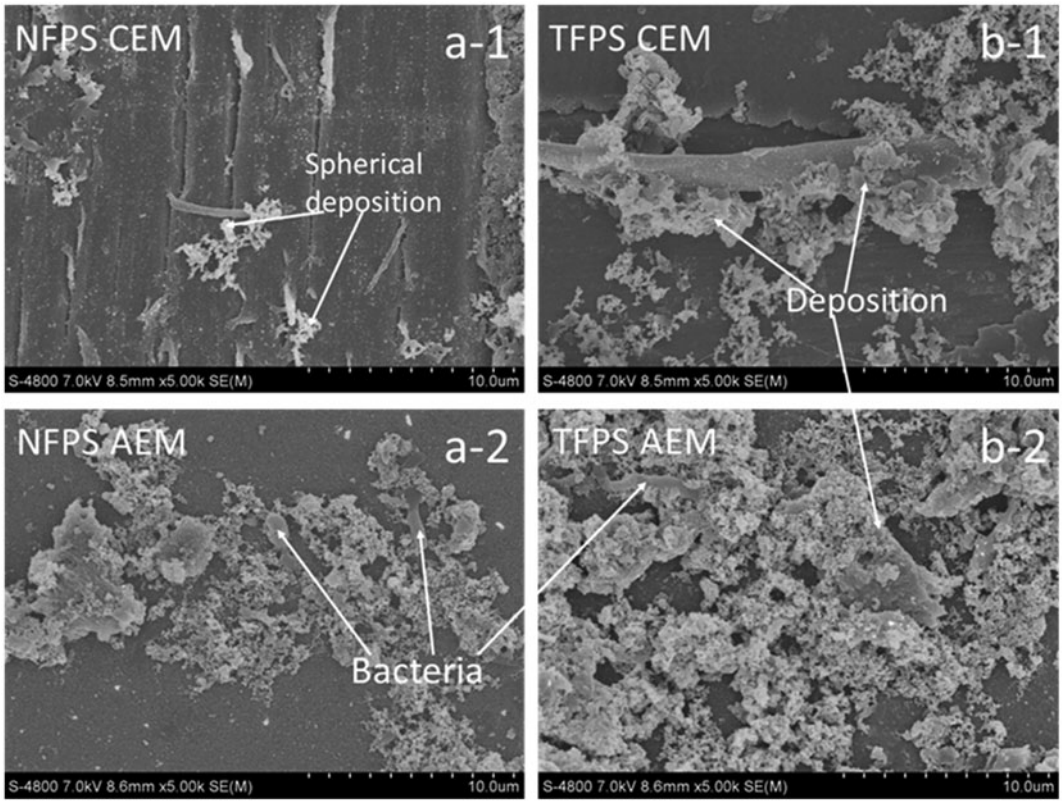

Fig. 10. SEM images (original magnification of 5,000×) of the CEM (a-1) and the AEM (a-2) under the NFPS, the CEM (b-1), and the AEM (b-2) under the TFPS.

Table 3
The elemental analysis of the surface of membranes (expressed as atomic percentage %)

Membrane (%)	a-1	b-1	a-2	b-2	1-AEM
Carbon	40.23	39.24	39.58	36.42	44.64
Oxygen	50.49	46.02	54.04	51.48	55.15
Magnesium	4.25	6.21	3.56	4.21	0
Calcium	3.86	5.26	1.32	3.54	0
Silicon	0.54	1.23	1.25	3.12	0
Phosphorus	0.63	2.04	0.25	1.23	0
Iron	0	0	0	0	0.21

be fouled by the positive mineral, because of the negative charge of the CEMs. Meanwhile, the concentration of the three inorganic ions is less on the membranes under NFPS, since it is hard channeling using the new spacers. According to the EDX-results (Table 3), both the contents of oxygen and silicon are higher on the AEMs than CEMs. This can be ascribed to that the negative charge on what these elements form. Moreover, the contents of iron are less at 1-AEM and iron are not detected on the other membranes through EDX (Table 3). The clean 1-AEM without iron demonstrates that 1-AEM is important in preventing the harmful iron into the dilute and brine compartments.

4. Conclusion

This research shows the importance of the spacers and how those affect the power density and the fouling of membranes in RED stack. In addition, we discuss the correlation between these spacers and power density obtained in RED stack. The use of new spacers and mixing electrolyte solution ($FeCl_3$ and $FeCl_2$) in RED leads to a tremendous increase in net power density and decrease in membrane fouling compared to the traditional spacers.

Another important aspect is that the spacers and the type of membranes do strongly influence on the rate and the degree of fouling. The types of fouling are also different because of the membranes with different charges in feed water. The organic pollution is mainly presented at the AEMs and the fouling of AEMs is more serious than the CEMs. The results demonstrated that the NFPS had less sensitive to fouling than the TFPS.

Acknowledgments

This work was financially supported by the public science and technology research funds projects of ocean (No. 201405035) and the public of marine renewable energy (No. GHME2013JS07).

References

[1] T. Xu, Ion exchange membranes: State of their development and perspective, J. Membr. Sci. 263 (2005) 1–29.
[2] G.Z. Ramon, B.J. Feinberg, E.M.V. Hoek, Membrane-based production of salinity-gradient power, Energy Environ. Sci. 4 (2011) 4423–4434.
[3] J.W. Post, J. Veerman, H.V.M. Hamelers, G.J.W. Euverink, S.J. Metz, K. Nymeijer, C.J.N. Buisman, Salinity-gradient power: Evaluation of pressure-retarded osmosis and reverse electrodialysis, J. Membr. Sci. 288 (2007) 218–230.
[4] J.W. Post, C.H. Goeting, J. Valk, S. Goinga, J. Veerman, H.V.M. Hamelers, Towards implementation of reverse electrodialysis for power generation from salinity gradients, Desalin. Water Treat. 16 (2010) 182–193.
[5] M.C. Hatzell, B.E. Logan, Evaluation of flow fields on bubble removal and system performance in an ammonium bicarbonate reverse electrodialysis stack, J. Membr. Sci. 446 (2013) 449–455.
[6] M. Hosenuzzaman, N.A. Rahim, J. Selvaraj, M. Hasanuzzaman, A.B.M.A. Malek, A. Nahar, Global prospects, progress, policies, and environmental impact of solar photovoltaic power generation, Renew. Sustain. Energy Rev. 41 (2015) 284–297.
[7] A. Daniilidis, D.A. Vermaas, R. Herber, K. Nijmeijer, Experimentally obtainable energy from mixing river water, seawater or brines with reverse electrodialysis, Renew. Energy 64 (2014) 123–131.
[8] J. Veerman, M. Saakes, S. Metz, G. Harmsen, Reverse electrodialysis: evaluation of suitable electrode systems, J. Appl. Electrochem. 40 (2010) 1461–1474.
[9] O.S. Burheim, F. Seland, J.G. Pharoah, S. Kjelstrup, Improved electrode systems for reverse electrodialysis and electrodialysis, Desalination 285 (2010) 147–152.
[10] J. Veerman, M. Saakes, S.J. Metz, G.J. Harmsen, Reverse electrodialysis: A validated process model for design and optimization, Chem. Eng. J. 166 (2011) 256–268.
[11] J. Veerman, M. Saakes, S.J. Metz, G.J. Harmsen, Reverse electrodialysis: Performance of a stack with 50 cells on the mixing of sea and river water, J. Membr. Sci. 327 (2009) 136–144.
[12] D.A. Vermaas, M. Saakes, K. Nijimeijer, Doubled power density from salinity gradients at reduced intermembrane distance, Environ. Sci. Technol. 45 (2011) 7089–7095.
[13] H. Strathmann, Ion-Exchange Membrane Separation Processes, Elsevier, Amsterdam, NL, 2004.
[14] P. Długołęcki, J. Dąbrowska, K. Nijmeijer, M. Wessling, Ion conductive spacers for increased power generation in reverse electrodialysis, J. Membr. Sci. 347 (2010) 101–107.
[15] D.A. Vermaas, M. Saakes, K. Nijmeijer, Enhanced mixing in the diffusive boundary layer for energy generation in reverse electrodialysis, J. Membr. Sci. 453 (2014) 312–319.
[16] E. Güler, R. Elizen, D.A. Vermaas, M. Saakes, K. Nijmeijer, Performance-determining membrane properties in reverse electrodialysis, J. Membr. Sci. 446 (2013) 266–276.
[17] R.D. Cusick, Y. Kim, B.E. Logan, Energy capture from thermolytic solutions in microbial reverse-electrodialysis cells, Science 335 (2012) 1474–1477.

[18] X. Luo, X. Cao, Y. Mo, K. Xiao, X. Zhang, P. Liang, X. Huang, Power generation by coupling reverse electrodialysis and ammonium bicarbonate: Implication for recovery of waste heat, Electrochem. Commun. 19 (2012) 25–28.
[19] A.M. Weiner, R.K. McGovern, J.H. Lienhard V, Increasing the power density and reducing the levelized cost of electricity of a reverse electrodialysis stack through blending, Desalination 369 (2015) 140–148.
[20] A.M. Weiner, R.K. McGovern, J.H. Lienhard V, A new reverse electrodialysis design strategy which significantly reduces the levelized cost of electricity, J. Membr. Sci. 493 (2015) 605–614.
[21] P. Dlugolecki, K. Nymeijer, S. Metz, M. Wessling, Current status of ion exchange membranes for power generation from salinity gradients, J. Membr. Sci. 319 (2008) 214–222.
[22] J. Veerman, J.W. Post, M. Saakes, S.J. Metz, G.J. Harmsen, Reducing power losses caused by ionic shortcut currents in reverse electrodialysis stacks by a validated model, J. Membr. Sci. 310 (2008) 418–430.
[23] J.N. Weinstein, F.B.J.W. LEITZ, Electric power from differences in salinity: The dialytic battery, Science 191 (1976) 557–559.
[24] Y. Mizutani, R. Yamane, H. Ihara, Studies of ion exchange membranes. XVI. The preparation of ion exchange membranes by the "paste method", Bull. Chem. Soc. Jpn. 36 (1963) 361–366.
[25] T. Sata, Preparation of ion exchange membranes, ion exchange membranes: Preparation, characterization, modification and application, The Royal Society of Chemistry, Cambridge, 2004, pp. 35–38.
[26] R.A. Tufa, E. Curcio, W. van Baak, J. Veerman, S. Grasman, E. Fontananova, G. Di Profio, Potential of brackish water and brine for energy generation by salinity gradient power-reverse electrodialysis (SGP-RE), RSC Adv. 4 (2014) 42617–42623.
[27] A. Tamburini, G. La Barbera, A. Cipollina, G. Micale, M. Ciofalo, CFD prediction of scalar tranport in thin channels for reverse electrodialysis, Desalin. Water Treat. 55 (2014) 3424–3445.